# Electronic g -tensors of solvated molecules using the polarizable continuum model

Zilvinas Rinkevicius, Lyudmyla Telyatnyk, Olav Vahtras, and Kenneth Ruud

Citation: The Journal of Chemical Physics **121**, 5051 (2004); doi: 10.1063/1.1779568
View online: http://dx.doi.org/10.1063/1.1779568
View Table of Contents: http://scitation.aip.org/content/aip/journal/jcp/121/11?ver=pdfcov
Published by the AIP Publishing

# Electronic *g*-tensors of solvated molecules using the polarizable continuum model

Zilvinas Rinkevicius, Lyudmyla Telyatnyk, and Olav Vahtras
*Laboratory of Theoretical Chemistry, The Royal Institute of Technology, SCFAB, SE-10691 Stockholm, Sweden*

Kenneth Ruud
*Department of Chemistry, University of Tromsø, N-9037 Tromsø, Norway*

(Received 15 April 2004; accepted 15 June 2004)

We present the implementation of density functional response theory combined with the polarizable continuum model (PCM), enabling first principles calculations of molecular *g*-tensors of solvated molecules. The calculated *g*-tensor shifts are compared with experimental *g*-tensor shifts obtained from electron paramagnetic resonance spectra for a few solvated species. The results indicate qualitative agreement between the calculations and the experimental data for aprotic solvents, whereas PCM fails to reproduce the electronic *g*-tensor behavior for protic solvents. This failure of PCM for protic solvents can be resolved by including into the model those solvent molecules which are involved in hydrogen bonding with the solute. The results for the protic solvents show that the explicit inclusion of the solvent molecules of the first solvation sphere is not sufficient in order to reproduce the behavior of the electronic *g*-tensor in protic solvents, and that better agreement with experimental data can be obtained by including the long-range electrostatic effects accounted for by the PCM approach on top of the explicit hydrogen-bonded complexes. © *2004 American Institute of Physics.* [DOI: 10.1063/1.1779568]

## I. INTRODUCTION

The electronic *g*-tensor, the hyperfine coupling, and the zero-field splitting (ZFS) tensors uniquely define the electron paramagnetic resonance (EPR) spectrum and therefore form key quantities in the search for information on the electronic structure of molecular radicals.[1,2] Due to the high reactivity and instability of open-shell species, experimental studies are usually carried out in inert environments such as frozen solutions and noble gas matrices or, in the case of bioradicals, in the native protein environment. However, for stable radicals such as nitric oxides, EPR measurements are commonly performed in solutions.[3–5] In all of these environments, the studied radical experiences interactions with the surrounding solvent or matrix molecules, which in turn are reflected in the observed spectra. Such environmental effects on the EPR spin-Hamiltonian parameters are well documented experimentally, and several empirical relations for the effect of a solvent or a matrix on the different spin-Hamiltonian parameters have been suggested.[3,6,7] There are, for example, well-known relationships between the nitrogen hyperfine coupling constants and the electronic *g*-tensors of nitric oxide radicals in various protic and aprotic solvents.[3]

Despite the experimental evidence for the importance of environmental effects in the analysis and interpretation of experimental EPR spectra,[3–8] the medium effects on the EPR parameters have attracted attention in theory and modeling only in recent years.[9–20] Whereas much theoretical effort has been recently devoted to the calculation of the medium effects on hyperfine coupling constants with successful applications to the study of organic radicals and transition metal complexes,[9,11,12,16–19] only a very limited number of calculations of these effects have been reported for electronic *g*-tensors[13–20] and ZFS tensors.[10] Therefore there is a need for developing methods that can reliably predict the medium effects on all EPR parameters. We have recently described an implementation of the polarizable continuum model (PCM) for the study of medium effects on ZFS tensors,[10] but no such implementation has yet been presented for the electronic *g*-tensor.[20] In this paper we intend to rectify this situation.

The effect of a solvent on the electronic *g*-tensor was established already in early experimental EPR spectroscopy works devoted to stable organic radicals.[3,4] The theoretical interpretation of the experimental results was provided by Stone,[21] who explained the changes in the electronic *g*-tensors of solvated radicals in terms of the perturbations arising from different types of solvent-solute interactions. This analysis was, however, based on an empirical model for the solvent-solute interactions using qualitative arguments. Only a few attempts have been made to investigate the electronic *g*-tensors of solvated radicals using modern quantum chemistry methods. Knüpling *et al.*[22] modeled the solute-solvent interaction of semiquinone anion radicals in frozen isotropic protic solvents by including point charges or explicit solvent molecules in model systems and by carrying out *g*-tensor calculations at the semiempirical UHF-PM3 level. Recently, Kaupp *et al.*[13] and Neyman *et al.*[15] investigated hydrogen bonding effects on the electronic *g*-tensors of various quinone anion radicals occurring in protic solvents using density functional theory (DFT) methods, where in the first work a conventional sum-over-states approach was employed in the evaluation of the electronic *g*-tensor and in the

 

second work a more sophisticated approach based on a relativistic two-component Kohn-Sham method was adopted. Similar investigations of hydrogen bonding effects on the electronic $g$-tensors of bioradicals have been carried out by Engström *et al.*[16,17] using *ab initio* multiconfiguration self-consistent field (MCSCF) and restricted open-shell Hartree-Fock (ROHF) linear response theory. All of these studies focused primarily on hydrogen bonding effects on the electronic $g$-tensors of radicals solved in protic solvents and the solute-solvent interaction was modeled by an explicit inclusion of solvent molecules in the calculations. In contrast, there is no theoretical investigation of medium effects on the electronic $g$-tensors of radicals in an aprotic solvent using modern quantum chemistry methods.[20] In this work we fill this gap in theoretical studies of EPR parameters by extending our electronic $g$-tensor formalism[23]—which is based on restricted DFT linear response theory—by including dielectric continuum effects using the Polarizable Continuum Model (PCM Ref. 24) to account for the solute-solvent interactions, which has proved successful in hyperfine coupling calculations of solvated radicals.[25] Here we will investigate the electronic $g$-tensor of two organic radicals, di-*t*-butyl nitric oxide and diphenyl nitric oxide, for which experimental data in protic and aprotic solvents exist, and rationalize the solvent dependence of the electronic $g$-tensors in terms of different solute-solvent interactions occurring in aprotic and protic solvents. In the case of the protic solvents, the validity of the previously employed models is assessed by explicitely including the hydrogen-bonded solvent molecules in the calculation, as well as the electrostatic interactions due to the presence of the bulk of the solvent.

## II. THEORY

### A. The electronic *g*-tensor of a molecule

Experimentally measured EPR spectra of molecules are analyzed using a phenomenological spin Hamiltonian and the electronic $g$-tensors as well as other spin-Hamiltonian parameters can readily be extracted from the experimental data through this analysis.[1,2] The electronic $g$-tensor appears in the spin Hamiltonian as a correction to the electronic Zeeman interaction bilinear in the effective electronic spin $\mathbf{S}$ and the external magnetic field induction $\mathbf{B}$, and can therefore be determined as the second derivative of the molecular electronic energy $\mathbf{E}$ with respect to these perturbations,

$$\mathbf{g}=\frac{1}{\mu_B}\frac{\partial^2 E}{\partial \mathbf{B}\partial \mathbf{S}}\bigg|_{\mathbf{B}=\mathbf{0},\mathbf{S}=\mathbf{0}}. \tag{1}$$

For molecules described by a Breit-Pauli Hamiltonian,[23,26–29] where spin and magnetic field as well as all other relativistic corrections are treated using perturbation theory, the molecular electronic $g$-tensor can be calculated to second order in the fine-structure constant $\alpha$ from the expression

$$\mathbf{g}=g_e\mathbf{1}+\Delta\mathbf{g}_{\mathrm{RMC}}+\Delta\mathbf{g}_{\mathrm{GC(1e)}}+\Delta\mathbf{g}_{\mathrm{GC(2e)}}+\Delta\mathbf{g}_{\mathrm{OZ/SO(1e)}}+\Delta\mathbf{g}_{\mathrm{OZ/SO(2e)}}. \tag{2}$$

In this equation, the first term is the free electron $g$-factor, which comes from the electronic Zeeman operator in the Breit-Pauli Hamiltonian, with the radiative corrections from quantum electrodynamics introduced into the Hamiltonian empirically. The next three terms originate from first-order perturbation theory applied to the Breit-Pauli Hamiltonian and are the mass-velocity and the one- and two-electron corrections to the electronic Zeeman effect, respectively. The last two terms are, respectively, the one- and two-electron corrections contributing to the electronic $g$-tensor in second order in perturbation theory as cross terms between the spin-orbit (SO) operators and the orbital Zeeman operator. All terms in Eq. (2) except the free electron $g$-factor value contribute to the electronic $g$-tensor shift $\Delta\mathbf{g}$, which accounts for the influence of the local electronic environment in the molecule on the unpaired electron(s) compared to the free electron. From the contributions to the $g$-tensor shift in Eq. (2), the first three terms are evaluated straightforwardly according to Eq. (1) from expectation values of the corresponding Breit-Pauli Hamiltonian operators, whereas the last two terms containing the SO corrections are considerably more demanding from a computational point of view, as they are defined in terms of second-order perturbation theory, i.e., they formally require knowledge of all relevant excited-state energies and wave functions in order for them to be computed correctly. The evaluation of these terms using *ab initio* or DFT methods is most often done using various kinds of approximate sum-over-states approaches[27] or response theory methods.[23,26,28,29]

In the present work, we follow our previous implementation of a method for electronic $g$-tensors calculations[23] based on spin-restricted DFT linear response theory. For the first-order perturbation theory contributions to the electronic $g$-tensor shift, we only include those terms that involve one-electron operators. The Cartesian $ab$ components of these tensors are

$$\Delta\mathbf{g}^{ab}_{\mathrm{RMC}}=-\frac{\alpha^2}{S}\langle 0|\sum_i p_i^2 s_{z,i}|0\rangle\delta^{ab}, \tag{3}$$

$$\Delta\mathbf{g}^{ab}_{\mathrm{GC(1e)}}=\frac{\alpha^2}{4S}\langle 0|\sum_i\sum_N\frac{Z_N}{r_{iN}^3}[(\mathbf{r}_{iN}\cdot\mathbf{r}_{iO})\delta^{ab}-\mathbf{r}^a_{iO}\mathbf{r}^b_{iN}]s_{z,i}|0\rangle, \tag{4}$$

where $p_i=-i\nabla_i$ is the canonical linear momentum of electron $i$, $s_{z,i}$ is the $z$ component of the spin operator of electron $i$, $\mathbf{r}_{iN}$ and $\mathbf{r}_{iO}$ are the position vectors of electron $i$ relative to nucleus $N$ and the magnetic gauge origin $O$, respectively. In the above equations $\Psi_0$ is chosen to be the ground-state wave function with maximum spin projection $S=M_S$. The two-electron gauge correction term $\Delta\mathbf{g}_{\mathrm{GC(2e)}}$ in Eq. (2) is neglected in our approach, since a two-electron operator cannot be evaluated using DFT unless it is approximated by an effective one-electron operator (for example, by a scaled one-electron gauge correction operator, see Ref. 28) or introduced by a noninteracting particles approximation, i.e., one uses Kohn-Sham orbitals in the evaluation of the two-electron density matrix. However, this term gives only a correction from a two-electron screening of the $\Delta\mathbf{g}_{\mathrm{GC(1e)}}$ contri-

bution and considering the smallness of the one-electron gauge correction term itself, the $\Delta\mathbf{g}_{\mathrm{GC(2e)}}$ can be neglected in calculations of the electronic $g$-tensor shifts without significant loss of accuracy.[27,29] The contributions arising from second-order perturbation theory, the one- and two-electron SO corrections, are in accordance with our previous work evaluated as linear response functions

$$\Delta\mathbf{g}^{ab}_{\mathrm{OZ/SO(1e)}}=\frac{1}{S}\langle\langle l^a_{iO};H^b_{\mathrm{SO(1e)}}\rangle\rangle_0, \tag{5}$$

$$\Delta\mathbf{g}^{ab}_{\mathrm{OZ/SO(2e)}}=\frac{1}{S}\langle\langle l^a_{iO};H^b_{\mathrm{SO(2e)}}\rangle\rangle_0, \tag{6}$$

where the spectral representation of the linear response function at zero frequency for two arbitrary operators $\hat{\mathbf{H}}_1$ and $\hat{\mathbf{H}}_2$ is given by

$$\langle\langle\hat{H}_1;\hat{H}_2\rangle\rangle_0 = \sum_{m>0}\frac{\langle 0|\hat{H}_1|m\rangle\langle m|\hat{H}_2|0\rangle+\langle 0|H_2|m\rangle\langle m|H_1|0\rangle}{E_0-E_m}. \tag{7}$$

In Eqs. (5) and (6), $l^a_{iO}$ is the Cartesian $a$ component of the angular momentum operator of electron $i$, and $H^b_{\mathrm{SO(1e)}}$ and $H^b_{\mathrm{SO(2e)}}$ are the Cartesian $b$ components of the one- and two-electron SO operators. The Cartesian $b$ component of the one-electron SO operator is defined as

$$H^b_{\mathrm{SO(1e)}}=\frac{\alpha^2}{2}\sum_i\sum_N\frac{Z_N l^b_{iN}}{\mathbf{r}^3_{iN}}s_{z,i}. \tag{8}$$

In this work we approximate the two-electron spin-orbit operator by an atomic mean field (AMFI) SO operator.[30] The AMFI-SO operator matrix elements for the $k$ and $l$ spin orbitals are obtained from the expression

$$\begin{aligned}H^b_{kl}=\sum_M^{mnf.orb} n_M[&\langle kM_\alpha|H^b_{SO(2e)}|lM_\alpha\rangle\\&+\langle kM_\beta|H^b_{SO(2e)}|lM_\beta\rangle-\langle kM_\alpha|H^b_{SO(2e)}|M_\alpha l\rangle\\&-\langle kM_\beta|H^b_{SO(2e)}|M_\beta l\rangle-\langle M_\alpha k|H^b_{SO(2e)}|lM_\alpha\rangle\\&-\langle M_\beta k|H^b_{SO(2e)}|lM_\beta\rangle].\end{aligned} \tag{9}$$

Here $n_M$ is the occupation number of orbital $M$, $M_p$ ($p=\alpha,\beta$) the partially occupied orbitals interacting with the electronic charge distribution, and $H^b_{SO(2e)}$ is the Cartesian $b$ component of the two-electron spin-orbit operator

$$H^b_{\mathrm{SO(2e)}}=-\frac{\alpha^2}{2}\sum_i\sum_{i\neq j}\frac{l^b_{ij}+2l^b_{ji}}{r^3_{ij}}s_{z,i}. \tag{10}$$

The AMFI-SO operator matrix element evaluated according to Eq. (9) is further simplified by neglecting all multicenter contributions, that is, the spin-orbit integrals are only calculated for individual atoms with full atomic symmetry imposed.[31] Previous experience with the AMFI-SO approximation in *ab initio* and DFT works devoted to electronic $g$-tensor calculations has been very encouraging and no significant problems with the accuracy of the AMFI-SO approximation have been reported.[23,27,29] Furthermore, we compared in our previous work the AMFI and scaled SO approximations[23] for the two-electron SO integrals, and found that the AMFI-SO approximation gives more accurate $g$-tensor results.

All calculations of the electronic $g$-tensors of the radicals included in this work were done using the methodology outlined above. However, before we turn to the calculations and the obtained results, let us briefly outline the principles of the PCM for the solvent effects on static properties in DFT linear response theory.

### B. The polarizable continuum model

Consider a molecular solute interacting with a solvent described as a homogeneous, dielectric continuum. The solute is placed in a molecule-shaped cavity embedded in the dielectric medium. The cavity is discretized into a set of small tesseraes, and the reaction field induced in the medium by the solute is described in terms of surface charges discretized on these tesseraes. Let us also assume that the solute is influenced by a static, external perturbation $\hat{P}$. The effective Hamiltonian for the solute is then given by

$$\hat{H}=\hat{H}_0+\hat{V}(\rho)+\hat{P}, \tag{11}$$

where $\hat{H}_0$ is the Kohn-Sham Hamiltonian of the isolated molecular system and $\hat{V}(\rho)$ is the solvent reaction field. The solvent reaction field describes the solute-solvent interaction and depends on the electron density $\rho$ of the solute. In the presence of only static perturbations, the solvent reaction field operator $\hat{V}$ can in second-quantization be written as

$$\hat{V}(\rho)=\sum_{\sigma\tau}\frac{1}{2}(\hat{J}_{\sigma\tau}+\hat{Y}_{\sigma\tau})E_{\sigma\tau}+\hat{X}_{\sigma\tau}(\rho)E_{\sigma\tau}, \tag{12}$$

where the summation runs over the molecular orbitals of the molecule, and $E_{\sigma\tau}$ are singlet creation operators

$$E_{\sigma\tau}=a^\dagger_{\sigma\alpha}a_{\tau\alpha}+a^\dagger_{\sigma\beta}a_{\tau\beta}. \tag{13}$$

In Eq. (12), $\hat{J}_{\sigma\tau}$ denotes the interaction of the electrons of the solute with the reaction field induced by the nuclei in solute, $\hat{Y}_{\sigma\tau}$ the interactions of the nuclei of the solute with the reaction field induced by the electrons of the solute, and $\hat{X}_{\sigma\tau}(\rho)$ denotes the interaction of the electrons of the solute with the reaction field induced by the electrons of the solute. The reaction field generated by the solvent is assumed to be in equilibrium with the electron density of the solute, that is, the time scale of the applied perturbation is longer than the solvent relaxation time.

The reaction field operators in Eq. (12) can in the integral equation formalism (IEF) of PCM be expressed as

$$\hat{J}_{\sigma\tau}=\hat{\mathbf{V}}^e_{\sigma\tau}\cdot\mathbf{q}^N, \tag{14}$$

$$\hat{Y}_{\sigma\tau}=\hat{\mathbf{V}}^N\cdot\mathbf{q}^e_{\sigma\tau}, \tag{15}$$

$$\hat{X}_{\sigma\tau}(\rho)=\sum_{\kappa\lambda}D_{\kappa\lambda}\hat{\mathbf{V}}^e_{\sigma\tau}\cdot\mathbf{q}^e_{\kappa\lambda}. \tag{16}$$

In these equations, $D_{\kappa\lambda}$ is the density matrix

$$D_{\kappa\lambda}=\langle 0|\mathbf{E}_{\kappa\lambda}|0\rangle, \tag{17}$$

$\hat{\mathbf{V}}^e_{\sigma\tau}$ and $\hat{\mathbf{V}}^N$ are vectors containing the potential at the different tesseraes due to the electrons and nuclei of the solute, respectively. $\mathbf{q}^N$ and $\mathbf{q}^e_{\sigma\tau}$ are vectors containing the polarization charges induced in the dielectric medium due to the nuclei and electrons of the solute, respectively. The charges are determined using the equation

$$\hat{\mathbf{q}}^{N/e} = \mathbf{C}^{-1}\hat{\mathbf{V}}^{N/e}, \tag{18}$$

where $\mathbf{C}$ is a non-Hermitian matrix that depends on the geometry of the cavity and the dielectric constant of the dielectric medium and has the dimension of the number of tesseraes squared. As the solvent operator depends on the electronic density of the solute, the optimization of the molecular energy and density is done in an iterative manner, and the energy of the solvated molecule is defined as the minimum of the free energy-functional

$$G = \langle 0|\hat{H} + \tfrac{1}{2}\hat{V}(\rho)|0\rangle. \tag{19}$$

A static, second-order molecular property such as the electronic $g$-tensor may be calculated as the second derivative of the free-energy functional $G$ with respect to the external magnetic field induction $\mathbf{B}$ and the effective spin $\mathbf{S}$,

$$g_{\alpha\beta} = \frac{d^2G}{d\mathbf{B}_\alpha d\mathbf{S}_\beta} = \frac{\partial^2 G}{\partial \mathbf{B}_\alpha \partial \mathbf{S}_\beta} + \frac{\partial^2 G}{\partial \mathbf{B}_\alpha \partial \lambda}\frac{\partial \lambda}{\partial \mathbf{S}_\beta}, \tag{20}$$

where $\lambda$ denotes the variational parameters of our DFT energy functional, which in the Kohn-Sham approximation of DFT correspond to unitary rotations among the Kohn-Sham orbitals.

In Eq. (20), the first term on the right-hand side represents the expectation value of the terms in $\hat{P}$ that are bilinear in the external magnetic field induction and the effective spin, that is, the first four terms of Eq. (2). The second term on the right-hand side involves the interaction between the magnetic field induction with the perturbed wave function due to the effective spin operator, and is a generalization of the sum-over-states expression in Eq. (7) to finite orbital bases. The perturbed wave function is determined by solving the linear response equation

$$\frac{\partial^2 G}{\partial \lambda^2}\frac{\partial \lambda}{\partial \mathbf{S}_\beta} = \frac{\partial^2 G}{\partial \lambda \partial \mathbf{S}_\beta}. \tag{21}$$

This equation is solved iteratively, in which the Hessian of the free-energy functional $\partial^2 G/\partial\lambda^2$ is contracted directly with a trial function $\sigma$, and compared with the right-hand side of the equation. The trial vector is set to the perturbed wave function $\partial\lambda/\partial\mathbf{S}_\beta$ at convergence. Since the solvent operator $\hat{V}(\rho)$ does not depend on the external perturbations, the only modifications required for introducing the contributions from the solvent are in the Hessian of the free-energy functional. Cammi *et al.* have previously described the required changes in the Hessian of the free-energy functional for frequency-dependent linear response functions.[32] In the case of a linear response function for a static perturbation, the Hessian of the free-energy functional can be written as

$$\frac{\partial^2 G}{\partial \lambda^2} = \frac{\partial^2 E}{\partial \lambda^2} + \frac{\partial^2 \mathbf{V}}{\partial \lambda^2}\cdot(\mathbf{q}^N + \mathbf{q}^{in}), \tag{22}$$

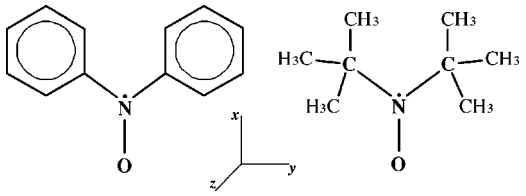


FIG. 1. The diphenyl nitric oxide (left) and the di-*t*-butyl nitric oxide (right) geometries and orientation of principal axes for electronic $g$-tensor.

where the first term on the right-hand side indicates the electronic Hessian of the vacuum Hamiltonian, and the second term is the correction term arising due to the presence of the dielectric continuum and involves the interaction of the surface charges with the second derivative of the electronic potentials at the tesseraes due to the electrons of the solute with respect to the orbital rotation parameters. We refer to Ref. 32 for more details.

## III. COMPUTATIONAL DETAILS

To illustrate the methodology described above for the calculation of electronic $g$-tensors of solvated molecules, we will present calculations for the di-*t*-butyl nitric oxide (N-I) and diphenyl nitric oxide (N-II) radicals (see Fig. 1), for which detailed experimental studies of the electronic $g$-tensors both in protic and aprotic solvents have been presented.[3,4] Geometry optimizations of both radicals have been carried out at the unrestricted B3LYP level using the 6-31$G(d,p)$ basis set in vacuum and in the solvents, carbon such as carbon tetrachloride (TCL), toluene, acetone, acetonitrile, methanol and water. All of these calculations have been performed using the GAUSSIAN 98 program.[33] All geometries of the solvated radicals have been optimized including the relevant PCM contributions to the molecular gradient. In the case of the protic solvents, methanol and water, additional complexes of the N-I and N-II radicals bound to one to three solvent molecules have been optimized in vacuum in order to model the hydrogen bonding between the solvent molecules and the solvated radicals. The optimized molecular structures of the radicals and their complexes were used in electronic $g$-tensor calculations both in vacuum and in different solvents. These calculations have been performed with a locally modified version of the DALTON quantum chemistry package,[34] in which the spin-restricted open-shell DFT linear response code has been modified to allow solvent effects to be accounted for using the PCM-IEF formalism.[35] All $g$-tensors calculations were performed using the BP86 (Refs. 36 and 37) and the B3LYP (Refs. 38–40) exchange-correlation functionals in the IGLO-II basis set.[41,42] This basis set is designed for accurate calculations of nuclear shieldings and electronic $g$-tensors. The use of the BP86 and B3LYP functionals was motivated by previous DFT studies of organic radical $g$-tensors,[23,28,29] whose calculations indicate that the BP86 functional has the best overall performance for organic radicals, but that the B3LYP functional in some particular systems provides more accurate results than the nonhybrid BP86 functional. In the PCM calculations, the following static dielectric constants were employed to de-

TABLE I. Electronic *g*-tensor of N-I in solution.[a]

| Geom.[b] solvent | B3LYP | | | | | | | | BP86 | | | | | | | | Expt.[c] |
|---|---|---|---|---|---|---|---|---|---|---|---|---|---|---|---|---|---|
| | Vacuum | | | | Solvent | | | | Vacuum | | | | Solvent | | | | |
| | $\Delta g_{xx}$ | $\Delta g_{yy}$ | $\Delta g_{zz}$ | $\Delta g_{iso}$ | $\Delta g_{xx}$ | $\Delta g_{yy}$ | $\Delta g_{zz}$ | $\Delta g_{iso}$ | $\Delta g_{xx}$ | $\Delta g_{yy}$ | $\Delta g_{zz}$ | $\Delta g_{iso}$ | $\Delta g_{xx}$ | $\Delta g_{yy}$ | $\Delta g_{zz}$ | $\Delta g_{iso}$ | $\Delta g_{iso}$ |
| Vacuum | −7 | 4135 | 7909 | 4012 | ⋯ | ⋯ | ⋯ | ⋯ | 11 | 3907 | 7233 | 3717 | ⋯ | ⋯ | ⋯ | ⋯ | ⋯ |
| TCL | −8 | 4100 | 7760 | 3951 | −34 | 4028 | 7581 | 3858 | 12 | 3884 | 7151 | 3682 | −22 | 3822 | 6994 | 3598 | 3751±20 |
| Toluene | −8 | 4097 | 7749 | 3946 | −34 | 4025 | 7563 | 3851 | 12 | 3882 | 7144 | 3679 | −22 | 3820 | 6981 | 3593 | 3741±10 |
| Acetone | −8 | 4048 | 7537 | 3859 | −36 | 3968 | 7338 | 3757 | 12 | 3850 | 7022 | 3628 | −24 | 3780 | 6846 | 3534 | 3721±50 |
| Acetonitrile | −8 | 4043 | 7519 | 3851 | −36 | 3964 | 7326 | 3751 | 13 | 3848 | 7011 | 3624 | −24 | 3777 | 6842 | 3531 | 3651±10 |
| Methanol | −8 | 4044 | 7520 | 3852 | −38 | 3962 | 7307 | 3743 | 12 | 3848 | 7013 | 3624 | −26 | 3774 | 6824 | 3524 | 3471±20 |
| Water | −8 | 4040 | 7505 | 3845 | −39 | 3959 | 7313 | 3744 | 12 | 3846 | 7003 | 3620 | −27 | 3771 | 6835 | 3526 | 3241±10 |

[a]Electronic *g*-tensor shift values are in ppm.
[b]Geometry used in calculations: vacuum or solvent optimized. Optimization carried out using B3LYP exchange-correlation functional.
[c]Experimental data taken from Ref. 3.

scribe the solvents: TCL, $\epsilon_0=2.228$; toluene, $\epsilon_0=2.379$; acetone, $\epsilon_0=20.7$; acetonitrile, $\epsilon_0=36.64$; methanol, $\epsilon_0=32.63$; and water, $\epsilon_0=78.39$. For the design of the cavity for the radicals, we follow the recommendations of Menucci *et al.*,[43] using a sphere radius of 1.7 Å for the carbon atoms, for the nitrogen atoms 1.6 Å, for the oxygen atoms 1.5 Å, for the CH groups in the N-II compound a single sphere of radius 1.9 Å was used, and finally a single sphere of radius 2.0 Å was used for the methyl groups in the N-I radical.

## IV. RESULTS AND DISCUSSION

### A. General trends in aprotic and protic solvents

The calculated electronic *g*-tensors in vacuum and selected solvents for the N-I and N-II compounds are summarized in Tables I and II. The electronic *g*-tensor shift $\Delta\mathbf{g}$ of both compounds is dominated by the $\Delta g_{zz}$ component, as expected due to the large spin-orbit contribution associated with the oxygen lone-pair orbital $(2p_y)$. The second largest $\Delta\mathbf{g}$ component is $\Delta g_{yy}$, which is approximately half the magnitude of $\Delta g_{zz}$. However, there is no relation between $\Delta g_{yy}$ and $\Delta g_{zz}$, as different sets of excited states contribute to their values. The smallest $\Delta\mathbf{g}$ component is $\Delta g_{xx}$, which is almost entirely determined by first-order contributions, $\Delta\mathbf{g}_{\mathrm{RMC}}$ and $\Delta\mathbf{g}_{\mathrm{GC(1e)}}$, as the second-order spin-orbit contribution [see Eq. (2)] is small for this $\Delta\mathbf{g}$ component. The ordering of the principal values of the *g*-tensor shift, $\Delta g_{zz} > \Delta g_{yy} > \Delta g_{xx}$, is independent of the solvent and the choice of geometry (vacuum or solvent optimized) used in a given calculation, as well as independent of the choice of exchange–correlation functional, BP86 or B3LYP. This is due to the strict separation of the excited states contributing to the different $\Delta\mathbf{g}$ components in the investigated nitric oxide compounds, N-I and N-II.

The isotropic *g*-tensor shift, $\Delta g_{iso}=1/3\mathrm{Tr}\Delta\mathbf{g}$, of the N-I compound evaluated for aprotic solvents follows the experimentally measured change in $\Delta g_{iso}$ going from TCL to acetonitrile (see Fig. 2) and decreases with increasing dielectric constant of the solvent. For N-II, the calculated results display a similar trend, but this can only be verified in an indirect manner, as experimental data are available only for TCL, methanol, and water. For the protic solvents, methanol and water, our results are for both compounds inconsistent with the experimental data: instead of a more pronounced decrease of $\Delta g_{iso}$ as observed in experiment, our calculated value for $\Delta g_{iso}$ in methanol is comparable to $\Delta g_{iso}$ in acetonitrile. This breakdown in the description of solvent effects in protic solvents is related to the use of PCM to model the solvent effects in our electronic *g*-tensor calculations, as this model is only capable of describing electrostatic interactions. In the case of protic solvents, hydrogen bonding between the solute and solvent molecules is responsible for the major part of the changes in the electronic structure of the solute, and

TABLE II. Electronic *g*-tensor of N-II in solution.[a]

| Geom.[b] solvent | B3LYP | | | | | | | | BP86 | | | | | | | | Expt.[c] |
|---|---|---|---|---|---|---|---|---|---|---|---|---|---|---|---|---|---|
| | Vacuum | | | | Solvent | | | | Vacuum | | | | Solvent | | | | |
| | $\Delta g_{xx}$ | $\Delta g_{yy}$ | $\Delta g_{zz}$ | $\Delta g_{iso}$ | $\Delta g_{xx}$ | $\Delta g_{yy}$ | $\Delta g_{zz}$ | $\Delta g_{iso}$ | $\Delta g_{xx}$ | $\Delta g_{yy}$ | $\Delta g_{zz}$ | $\Delta g_{iso}$ | $\Delta g_{xx}$ | $\Delta g_{yy}$ | $\Delta g_{zz}$ | $\Delta g_{iso}$ | $\Delta g_{iso}$ |
| Vacuum | −124 | 3348 | 8318 | 3847 | ⋯ | ⋯ | ⋯ | ⋯ | −157 | 2991 | 7611 | 3482 | ⋯ | ⋯ | ⋯ | ⋯ | ⋯ |
| TCL | −129 | 3296 | 8026 | 3731 | 42 | 3091 | 7586 | 3573 | −160 | 2953 | 7401 | 3398 | 63 | 2769 | 6990 | 3274 | 3401±10 |
| Toluene | −130 | 3293 | 8005 | 3723 | 44 | 3085 | 7534 | 3558 | −161 | 2950 | 7386 | 3392 | 65 | 2764 | 6953 | 3261 | ⋯ |
| Acetone | −136 | 3225 | 7645 | 3578 | 46 | 3012 | 7184 | 3414 | −164 | 2899 | 7122 | 3286 | 68 | 2708 | 6696 | 3157 | ⋯ |
| Acetonitrile | −135 | 3219 | 7617 | 3567 | 47 | 3004 | 7145 | 3398 | −165 | 2895 | 7102 | 3277 | 69 | 2701 | 6665 | 3145 | ⋯ |
| Methanol | −136 | 3220 | 7622 | 3569 | 44 | 3016 | 7224 | 3428 | −165 | 2896 | 7105 | 3279 | 66 | 2710 | 6741 | 3172 | 3181±10 |
| Water | −136 | 3216 | 7597 | 3559 | 46 | 3007 | 7180 | 3411 | −166 | 2893 | 7087 | 3271 | 68 | 2703 | 6704 | 3158 | 2761±10 |

[a]Electronic *g*-tensor shift values are in ppm.
[b]Geometry used in calculations: vacuum or solvent optimized. Optimization carried out using B3LYP exchange-correlation functional.
[c]Experimental data taken from Ref. 4.

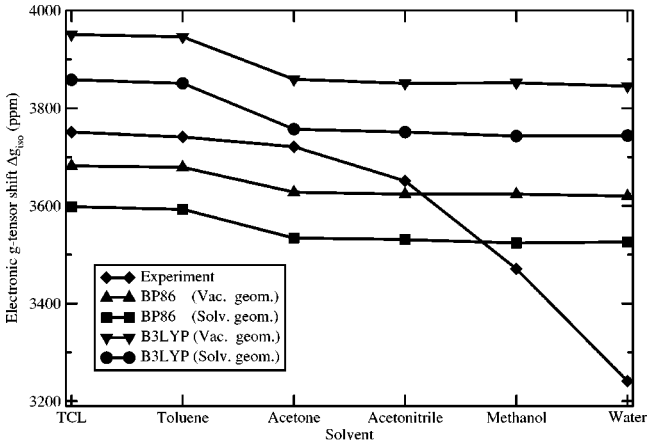


FIG. 2. The experimentally determined isotropic $g$-tensor shift and corresponding theoretically evaluated isotropic $g$-tensor shift dependence on the employed solvent.

this effect is not accounted for by PCM. The limitations of PCM for protic solvents are well known, and can be overcome by the explicit introduction of solvent molecules forming hydrogen bonds with the solute in the calculations. The hydrogen bonding effects and their interplay with the electrostatic effects accounted for by PCM will be discussed in detail for water and methanol solutions of N-I and N-II in the following section. Here, we will limit ourselves to a discussion of the influence of aprotic and protic solvents on the electronic $g$-tensor shifts of N-I and N-II as described by PCM.

For both compounds, the largest component of $\Delta\mathbf{g}$, $\Delta g_{zz}$, which almost exclusively determines the behavior of $\Delta g_{iso}$, decreases going from TCL to water. This is primarily due to the blueshift of the $n-\pi_{SOMO}$ excitation energy, i.e., it is caused by an increase of the denominator of the dominating second-order contribution to $\Delta g_{zz}$ arising from this virtual excitation. The solvent-induced blueshift of the $n-\pi_{SOMO}$ excitation energy calculated with the BP86 functional for N-I (vacuum geometry) is 8 $cm^{-1}$ for toluene, 164 $cm^{-1}$ for acetone, 179 $cm^{-1}$ for acetonitrile, 176 $cm^{-1}$ for methanol, and 188 $cm^{-1}$ for water, to be compared to the calculated $n-\pi_{SOMO}$ excitation energy of 20 994 $cm^{-1}$ in TCL. These $n-\pi_{SOMO}$ blueshifts of the excitation energy show the same pattern as the experimentally obtained blue shifts observed for the aprotic solvents, where the blueshifts are 110 $cm^{-1}$ for toluene, 210 $cm^{-1}$ for acetone, and 430 $cm^{-1}$ for acetonitrile, but show significant deviations for protic solvents, where the experimental blueshifts are 1010 $cm^{-1}$ for methanol and 2010 $cm^{-1}$ for water. For N-II (vacuum geometry, BP86 functional), the blueshift of the $n-\pi_{SOMO}$ excitation energy is more pronounced, and is 14 $cm^{-1}$ for toluene, 5250 $cm^{-1}$ for acetone, 5213 $cm^{-1}$ for acetonitrile, 5220 $cm^{-1}$ for methanol, and 5187 $cm^{-1}$ for water compared to the calculated $n-\pi_{SOMO}$ excitation energy of 18 029 $cm^{-1}$ in TCL. However, for the N-II compound, the $n-\pi_{SOMO}$ excitation transition is very weak and vanishes in an intense $\pi-\pi^*$ transition, and thus cannot be extracted accurately from experimental spectra, i.e., no reliable experimental data for the blueshifts of the $n-\pi_{SOMO}$ excitation are available. A closer inspection of the calculated excitation energies for N-I and N-II indicates that the experimental blueshift for N-I cannot be qualitatively reproduced for acetonitrile, methanol, and water. A similar situation can be expected for N-II, where the blueshift decreases instead of increase when going from methanol to water as would otherwise have been expected. Therefore, these inconsistencies in the calculated blueshifts lead to only slightly different values for $\Delta g_{zz}$ for these solvents both in N-I and N-II. However, although the dominating effect in the decrease of $\Delta g_{zz}$ is due to this blueshift, the changes in the spin-orbit and angular momentum operator matrix elements caused by the redistribution of the unpaired electron density in various solvents cannot be neglected either.

The second largest component of the electronic $g$-tensor shift, $\Delta g_{yy}$, shows only a small decrease in its value both in N-I and N-II when going from TCL to water, due to the more modest blueshift of the excitation energies contributing to this $\Delta\mathbf{g}$ component. The smallest component of $\Delta\mathbf{g}$, namely $\Delta g_{xx}$, is in both radicals small and mainly determined by the first-order contributions, which are only affected by the redistribution of the unpaired electron density caused by the solvent and, consequently, changes only little in different solvents. In summary, the isotropic $g$-tensor shift, which is dominated by the behavior of the $\Delta g_{zz}$ component, decreases going from TCL to water for both compounds, but the calculations cannot reproduce the marked decrease in $\Delta g_{iso}$ in both compounds for the protic solvents, due to the limitations of PCM.

The geometries of N-I and N-II used in the calculations of the electronic $g$-tensors were optimized in vacuum and in the investigated solvents in order to assess the effect of solvation on the geometrical parameters and in turn on the electronic $g$-tensor values for the two compounds. Overall, the bond distances in both compounds, including the N—O and N—C bonds, are only slightly affected (0.001–0.003 Å) by the solvent. However, a more pronounced distortion of bond angles and dihedral angles is observed when comparing vacuum- and solvent-optimized structures. The most important geometrical parameter is $\angle$CNC, which is responsible for the orientation of the —$C(CH)_3$ group in N-I and the —$C_6H_5$ group in N-II with respect to the oxygen lone-pair orbital which largely determines $\Delta g_{zz}$. This angle decreases upon solvation by about 3° and 1.4° with respect to the vacuum-optimized geometry in N-I and N-II, respectively. The changes in the $\angle$CNC when going from one solvent to another are in the order of 0.05°–0.1° for both compounds, indicating small differences between the —$C(CH)_3$ and —$C_6H_5$ arrangements in different solvents. $\Delta g_{iso}$ decreases by about 100 ppm (BP86, B3LYP) in N-I and by about 110–130 ppm (BP86) or 150–170 ppm (B3LYP) for N-II when solvent-optimized geometries are used instead of vacuum-optimized geometries. The solvent-induced distortion of the vacuum geometry affects all components of $\Delta\mathbf{g}$ in both compounds, with the largest decrease observed in $\Delta g_{zz}$ because of the sensitivity of this component to the oxygen lone-pair environment and its orientation in the molecule. The other components of the electronic $g$-tensor shift show more moderate changes, with $\Delta g_{yy}$ decreasing and $\Delta g_{xx}$ changing sign

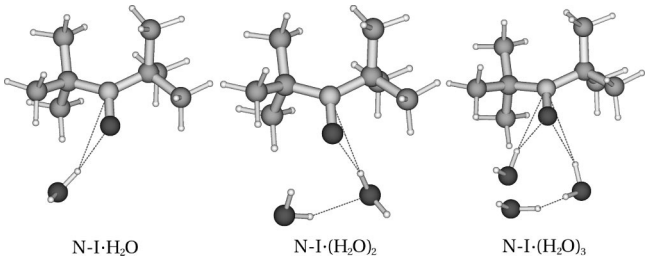


FIG. 3. Di-*t*-butyl nitric oxide complexes with *n* water molecules ($n=1,2,3$).

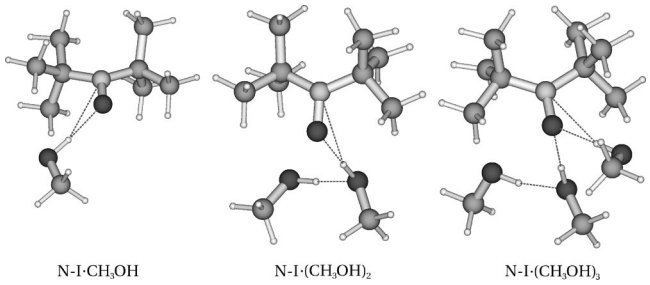


FIG. 5. Di-*t*-butyl nitric oxide complexes with *n* methanol molecules ($n=1,2,3$).

and increasing slightly for N-I (BP86) and N-II (BP86, B3LYP). Comparing $\Delta g_{iso}$ for N-I to the experimentally observed shifts for aprotic solvents, the best agreement is obtained with the BP86 functional at the vacuum-optimized geometry. The $\Delta g_{iso}$ values obtained with the B3LYP functional at the solvent-optimized geometry show deviations from experiment comparable to the deviations observed for the BP86 values at the solvent-optimized geometry, but approaches the experimental data from above, whereas the BP86 values are below the experimental data (see Fig. 2). The worst agreement between the calculated and experimental data is obtained with the B3LYP functional at the vacuum geometry. These results are in line with previous work on DFT calculations of electronic *g*-tensors, where it has been shown that for organic compounds,[23,28,29] the hybrid exchange-correlation functionals do not improve the results obtained with GGA functionals, and that the BP86 functional gives the best overall agreement with experiment. Our limited calculations of the electronic *g*-tensor for N-I suggest a somewhat better performance at the vacuum-optimized geometry, but more extensive and systematic investigations are required in order to assess the importance of the solvent-induced geometrical distortions in electronic *g*-tensor calculations.

### B. Hydrogen bonding effects in protic solvents

In protic solvents, the solute forms hydrogen bonds with surrounding solvent molecules and the short-range interactions between the solute and solvent molecules influence the electronic structure of the solute and consequently affect its electronic *g*-tensor. As already noted, PCM is not capable of properly accounting for hydrogen bonding effects, and therefore we explicitly included methanol or water molecules by building molecular complexes and in this way accounting for the strong hydrogen bonding between the NO groups of the N-I and N-II compounds and the solvent molecules. Various models for the N-I and N-II compounds in methanol and water have been studied, containing from one to three solvent molecules. The complexes were optimized in vacuum using the B3LYP functional. The complexes of N-I and N-II with water are shown in Figs. 3 and 4, and the complexes with methanol are shown in Figs. 5 and 6. The major difference between these different structures is that in the case of N-I, the second solvent molecule forms a hydrogen bond with another solvent molecule [see the N-I·$(H_2O)_2$ and N-I·$(CH_3OH)_2$ complexes], whereas the second solvent molecule form a bond directly with the NO group of the solute in the N-II complexes. Monte Carlo simulations of a water solution of $(CH_3)_2NO$ (Ref. 44), which has a similar structure as N-I, indicate that about 1.52 water molecules participate in hydrogen bonding with the solute, and the obtained structures to some extent resemble our structure of the N-I compound complex with three water molecules. The B3LYP-optimized structures of N-I with solvent molecules are not quite satisfactory and further investigations with more sophisticated methods appear to be required in order to elucidate the most stable structures of N-I in methanol and water more accurately. The hydrogen bond lengths between the NO group in N-I and N-II and the methanol molecules vary from 1.77 Å to 1.85 Å, and from 1.82 Å to 1.94 Å, respectively, depending on the number of solvent molecules included in the model. Similarly, hydrogen bond lengths in the water complexes vary between 1.84 and 1.98 Å in the N-I complexes and between 1.85 and 1.99 Å in the N-II complexes. Hydrogen bonding affects the most important

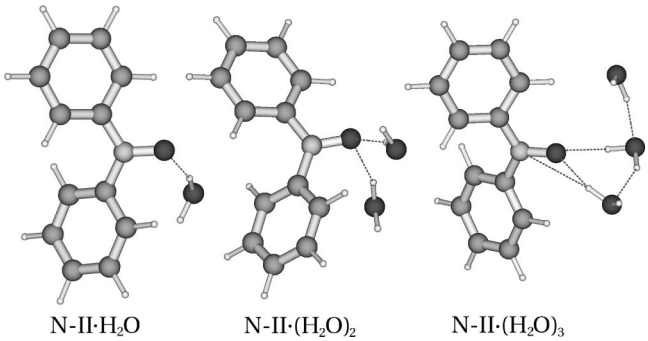


FIG. 4. Diphenyl nitric oxide complexes with *n* water molecules ($n=1,2,3$).

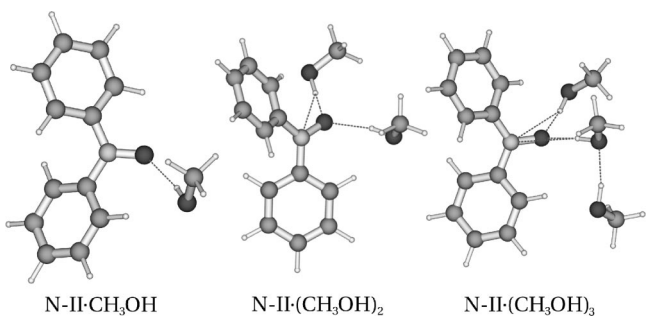


FIG. 6. Diphenyl nitric oxide complexes with *n* methanol molecules ($n=1,2,3$).

TABLE III. Electronic $g$-tensor of N-I in protic solvents.[a]

| Environment[b] complex | B3LYP | | | | | | | | BP86 | | | | | | | | Expt.[c] |
|---|---|---|---|---|---|---|---|---|---|---|---|---|---|---|---|---|---|
| | Vacuum | | | | Solvent | | | | Vacuum | | | | Solvent | | | | |
| | $\Delta g_{xx}$ | $\Delta g_{yy}$ | $\Delta g_{zz}$ | $\Delta g_{iso}$ | $\Delta g_{xx}$ | $\Delta g_{yy}$ | $\Delta g_{zz}$ | $\Delta g_{iso}$ | $\Delta g_{xx}$ | $\Delta g_{yy}$ | $\Delta g_{zz}$ | $\Delta g_{iso}$ | $\Delta g_{xx}$ | $\Delta g_{yy}$ | $\Delta g_{zz}$ | $\Delta g_{iso}$ | $\Delta g_{iso}$ |
| Methanol | | | | | | | | | | | | | | | | | |
| N-I | −7 | 4135 | 7909 | 4012 | −8 | 4044 | 7520 | 3852 | 11 | 3907 | 7233 | 3717 | 12 | 3848 | 7013 | 3624 | |
| N-I·$CH_3OH$ | −86 | 3737 | 6963 | 3538 | −87 | 3668 | 6696 | 3426 | −71 | 3544 | 6477 | 3317 | −71 | 3495 | 6318 | 3247 | |
| N-I·$(CH_3OH)_2$ | −94 | 3662 | 6877 | 3482 | −93 | 3611 | 6685 | 3401 | −70 | 3492 | 6483 | 3302 | −70 | 3455 | 6372 | 3252 | |
| N-I·$(CH_3OH)_3$ | −108 | 1174 | 1014 | 693 | −109 | 1216 | 1023 | 710 | −88 | 1124 | 951 | 662 | −90 | 1168 | 958 | 678 | 3471±20 |
| Water | | | | | | | | | | | | | | | | | |
| N-I | −7 | 4135 | 7909 | 4012 | −8 | 4040 | 7505 | 3845 | 11 | 3907 | 7233 | 3717 | 12 | 3846 | 7003 | 3620 | |
| N-I·$H_2O$ | −77 | 3780 | 7034 | 3579 | −77 | 3705 | 6772 | 3466 | −63 | 3587 | 6555 | 3360 | −65 | 3534 | 6401 | 3290 | |
| N-I·$(H_2O)_2$ | −79 | 3667 | 6658 | 3415 | −78 | 3624 | 6487 | 3344 | −55 | 3485 | 6278 | 3236 | −58 | 3458 | 6176 | 3192 | |
| N-I·$(H_2O)_3$ | −94 | 3568 | 6531 | 3335 | −96 | 3528 | 6390 | 3274 | −69 | 3400 | 6202 | 3178 | −75 | 3371 | 6125 | 3140 | 3241±10 |

[a]Electronic $g$-tensor shift values are in ppm.

[b]Geometry used in calculations is optimized in vacuum using B3LYP exchange-correlation functional. The calculations of $g$-tensor are carried out in vacuum (environment-vacuum) and in protic solvents (environment-solvent).

[c]Experimental data taken from Ref. 4.

geometrical parameters of the N-I and N-II compounds, namely the N—O and N—C bond lengths, which directly influence the lone-pair electron in both molecules. The N—O bond length changes by ≈0.003 Å in both methanol and water for N-I. In the case of N-II, even more pronounced changes are observed: 0.008 Å in methanol and 0.007 Å in water. The influence of hydrogen bonding on the N—C bond lengths in the different N-I and N-II complexes is less pronounced, whereas ∠CNC is much more affected and changes by 1.2°–2.6°. We do not discuss the structures of the N-I and N-II complexes with methanol and water molecules in more detail here, focusing instead on the effects of combining the molecular complexes with PCM in the calculation of the electronic $g$-tensor of the solvated N-I and N-II molecules.

The electronic $g$-tensor results for the hydrogen bonded complexes of N-I with water and methanol are summarized in Table III. Two kinds of calculations have been performed: calculations of the electronic $g$-tensor of the complexes in vacuum and in a dielectric medium with the same dielectric constant as the solvent molecules. The calculations of the methanol and water complexes of N-I (see Fig. 3 and Fig. 4) indicate that the best agreement with experiment is obtained using the B3LYP functional with the hydrogen bonding in methanol represented by the N-I·$CH_3OH$ complex, and hydrogen bonding in water represented by the N-I·$(H_2O)_3$ complex. The selection of the N-I·$(H_2O)_3$ complex as most representative is not only due to the fact that this complex gives the best agreement with experiment, but also due to the close correspondence between the geometrical structure of the N-I·$(H_2O)_3$ complex and the structures obtained in the Monte Carlo simulations of $(CH_3)_2NO$ in water by Yagi *et al.*[44] $\Delta g_{iso}$ results calculated using the BP86 functional have worse agreement with experiment than the B3LYP results for the N-I·$CH_3OH$ and N-I·$(H_2O)_3$ complexes. Even though BP86 performs better in comparison to experiment than B3LYP for the N-I·$(H_2O)_2$ complex, we favor the N-I·$CH_3OH$ and N-I·$(H_2O)_3$ complexes. The calculated solvent-induced decrease of $\Delta g_{iso}$ for N-I is 586 ppm in methanol and 738 ppm in water [see Table III, B3LYP results for N-I·$CH_3OH$ and N-I·$(H_2O)_3$], with $\Delta g_{iso}$ of N-I evaluated in vacuum (4012 ppm) used as reference. In methanol, ≈80% (477 ppm) of the solvent-induced decrease of $\Delta g_{iso}$ is due to the hydrogen bonding and the remaining 109 ppm is due to the long-range electrostatic interactions between the solute and the solvent. The situation is slightly different in water due to the much stronger hydrogen bonds formed by water, and hydrogen bonding accounts in this case for 91% (677 ppm) of the total solvent-induced decrease in the isotropic $g$-tensor shift of 738 ppm. As was the case for the PCM calculations, the explicit inclusion of hydrogen bonding mostly affects the largest component of $\Delta g_{iso}$, namely $\Delta g_{zz}$, mainly through delocalization of the lone pair and a redistribution of the unpaired electron density caused by the hydrogen bond formation. To summarize the calculations of the electronic $g$-tensor shifts of N-I in the protic solvents methanol and water: (1) Explicit inclusion of the solvent molecules that are hydrogen bonded to the solute is crucial for reliable calculations of the electronic $g$-tensor of molecules solved in protic solvents; (2) Long-range electrostatic effects cannot be neglected in protic solvents and should be accounted for using, for instance, PCM. This is particularly important for protic solvents that only form relatively ''weak'' hydrogen bonds.

The results of the electronic $g$-tensor calculations for the complexes of N-II with methanol and water are tabulated in Table IV. Best agreement between the calculated isotropic $g$-tensor shift of N-II and experiment is obtained for the N-II·$CH_3OH$ and N-II·$(H_2O)_2$ complexes, both using the B3LYP and the BP86 functional. For methanol, better agreement with experiment is obtained with the B3LYP functional, while the BP86 results show better agreement with experiment for water. Contrary to N-I, where the best model of the water solution was found to be the N-I·$(H_2O)_3$ complex, for N-II the complex with two water molecules directly bonded to the NO group gave the best results compared to experiment. The calculated decrease in the isotropic electronic $g$-tensors induced by the solvent, taking $\Delta g_{iso}$ in

TABLE IV. Electronic $g$-tensor of N-II in protic solvents.[a]

| Environment[b] complex | B3LYP | | | | | | | | BP86 | | | | | | | | Expt.[c] |
|---|---|---|---|---|---|---|---|---|---|---|---|---|---|---|---|---|---|
| | Vacuum | | | | Solvent | | | | Vacuum | | | | Solvent | | | | |
| | $\Delta g_{xx}$ | $\Delta g_{yy}$ | $\Delta g_{zz}$ | $\Delta g_{iso}$ | $\Delta g_{xx}$ | $\Delta g_{yy}$ | $\Delta g_{zz}$ | $\Delta g_{iso}$ | $\Delta g_{xx}$ | $\Delta g_{yy}$ | $\Delta g_{zz}$ | $\Delta g_{iso}$ | $\Delta g_{xx}$ | $\Delta g_{yy}$ | $\Delta g_{zz}$ | $\Delta g_{iso}$ | $\Delta g_{iso}$ |
| Methanol | | | | | | | | | | | | | | | | | |
| N-II | −124 | 3348 | 8318 | 3847 | −136 | 3220 | 7622 | 3569 | −157 | 2991 | 7611 | 3482 | −165 | 2896 | 7105 | 3279 | |
| N-II·$CH_3OH$ | −13 | 2937 | 7171 | 3369 | 20 | 2837 | 6646 | 3162 | 50 | 2655 | 6679 | 3128 | 44 | 2572 | 6276 | 2964 | |
| N-II·$(CH_3OH)_2$ | −8 | 2751 | 6556 | 3100 | −10 | 2659 | 6116 | 2921 | 82 | 2537 | 6260 | 2959 | 57 | 2445 | 5907 | 2803 | |
| N-II·$(CH_3OH)_3$ | −8 | 886 | 5782 | 2195 | −81 | 872 | 5443 | 2078 | −60 | 820 | 5623 | 2128 | −84 | 849 | 5278 | 2039 | 3181±10 |
| Water | | | | | | | | | | | | | | | | | |
| N-II | −124 | 3348 | 8318 | 3847 | −136 | 3216 | 7597 | 3559 | −157 | 2991 | 7611 | 3482 | −166 | 2893 | 7087 | 3271 | |
| N-II·$H_2O$ | −90 | 2935 | 7225 | 3383 | 12 | 2782 | 6541 | 3108 | −21 | 2636 | 6697 | 3110 | 15 | 2504 | 6175 | 2898 | |
| N-II·$(H_2O)_2$ | −51 | 2739 | 6555 | 3096 | −10 | 2650 | 6151 | 2933 | 31 | 2480 | 6204 | 2905 | 34 | 2398 | 5888 | 2773 | |
| N-II·$(H_2O)_3$ | −18 | 2684 | 6447 | 3038 | −19 | 2659 | 6280 | 2974 | 40 | 2424 | 6128 | 2864 | 33 | 2405 | 5998 | 2812 | 2761±10 |

[a]Electronic $g$-tensor shift values are in ppm.
[b]Geometry used in calculations is optimized in vacuum using B3LYP exchange-correlation functional. The calculations of $g$-tensor are carried out in vacuum (environment-vacuum) and in protic solvents (environment-solvent).
[c]Experimental data taken from Ref. 4.

vacuum as a reference, is 685 ppm in methanol and 914 ppm in water (B3LYP results in solvent, see Table IV) and is larger than the results obtained for N-I due to the stronger hydrogen bonds formed between methanol or water with the N-II molecule. The hydrogen bonding accounts for ≈70% (478 ppm) of the total solvent-induced decrease of $\Delta g_{iso}$ in methanol (685 ppm), and in the case of water accounts for about 82% (751 ppm) of the total $\Delta g_{iso}$ solvent shift (914 ppm). In the case of the N-II compound, the long-range electrostatic effects described by PCM give more significant contributions to the total solvent-induced $\Delta g_{iso}$ decrease compared to the N-I molecule due to the presence of the $\pi$-electron system, which is easily polarized by the solvent. As for N-I, the largest solvent-induced decrease in $\Delta g_{iso}$ is observed in the $\Delta g_{zz}$ component. When comparing the electronic $g$-tensor behavior of the N-I and N-II compounds in protic solvents, a similar pattern in the decrease of the electronic $g$-tensor shifts is observed, but changes due to solvation in protic solvents are more pronounced in the N-II compound. This slight difference in the behavior of the N-I and N-II compounds can be attributed to the larger hydrogen-bond forming ability of the N-II compound and the extended $\pi$-electron system in this molecule, which is easily polarized in solution.

Calculated $g$-tensor shifts of the N-I and N-II complexes with three methanol molecules (see Table III–IV) significantly deviate from general trends observed in the N-I and N-II complexes with methanol and water molecules and this discrepancy in our calculations can be attributed to the artificial geometrical structure of these complexes. Therefore, reliable geometrical structure of solute-solvent model is crucial in order to obtain meaningful results, when one explicitly includes solvent molecules into the model used in quantum chemical calculations.

## V. CONCLUSIONS

This paper has presented the development, implementation and applications of an approach for calculating electronic $g$-tensors that is capable of accounting for environmental effects caused by a solvent as described by a polarizable continuum model. The electronic $g$-tensor formalism is based on open-shell spin-restricted DFT linear response theory, which has previously been successfully applied to the evaluation of the electronic $g$-tensors of organic radicals in vacuum. The methodology presented here allows us to describe, within the limits of the PCM approach, the environmental effects on the $g$-tensor of a solute and enables a more realistic modeling of radicals in aprotic solvents as well as protein environments.

An exploratory investigation of the behavior of the electronic $g$-tensor in aprotic and protic solvents of diphenyl nitric oxide and di-$t$-butyl nitric oxide indicates that the approach is capable of qualitative predictions of the changes in the electronic $g$-tensor of the investigated compounds in aprotic solvents. However, the description of the changes in the electronic $g$-tensors caused by protic solvents is poor, due to the well-known limitations of the PCM approach in modeling hydrogen bonding effects. These are, namely, the dominating contributions to the changes in the $g$-tensors in protic solvents. The decrease in the electronic $g$-tensor shift of N-I and N-II in solvent as observed experimentally as well as in our calculations, is mainly due to the decrease of the largest $\Delta g_{zz}$ component, which primarily is due to the blueshift of the $n$-$\pi^*$ excitation energy. Our calculations indicate only minor changes in the matrix elements of the spin-orbit and angular momentum operators which are involved in the leading second-order spin-orbit contribution to $\Delta\mathbf{g}$. Redistribution of the unpaired electron density is therefore negligible in our calculations. Our approach for evaluating the electronic $g$-tensor in aprotic solvents is capable of providing a qualitatively correct picture of the changes in the electronic $g$-tensor, and a further improvement in the accuracy of the calculation will be closely associated with the improvement in the changes in the excitation energies upon solvation, as the calculated $n$-$\pi^*$ excitation energy blueshifts are not satisfactory in comparison to the experiment. It should, however, be noted that we used an equilibrium solvation scheme when calculating the excitation energies (since this is the

most relevant approximation for the case of static properties such as electronic $g$-tensors, and thus exact agreement with experiment for the excitation energies cannot be hoped for, since this would require the use of a nonequilibrium solvation scheme[45]).

In protic solvents, the description of solvent effects by PCM is entirely unsatisfactory, as observed in our calculations of the electronic $g$-tensors of the N-I and N-II compounds in methanol and water. The way to overcome this limitation of the PCM approach is to explicitly include solvent molecules, which form hydrogen bonds with the solute and to calculate the electronic $g$-tensors of these complexes in vacuum. In this work we have demonstrated that this methodology can be further improved by also including long-range electrostatic effects via the PCM approach in addition to the explicit hydrogen-bonded complexes. Indeed, the long-range electrostatic effects can be significant (accounting for almost 30% of the solvent-induced shift of $\Delta g_{iso}$ in N-II), especially in molecules with easily polarizable extended $\pi$-electron systems. In calculations of electronic $g$-tensors we therefore recommend to include the solvent molecules in the first solvation sphere, which form strong hydrogen bonds with solute, in the model, and treat the remaining solvent effect by the PCM approach. This approach can be particularly rewarding in investigations of bioradicals in their native protein environment and the performance of this model for calculations of electronic $g$-tensors in bioradicals will be investigated in future works.

## ACKNOWLEDGMENTS

Z.R. acknowledges the support from the EU network ''Molecular Properties and Molecular Materials'' (MOLPROP, Contract No. HPRN-CN-2000-0013). O.V. acknowledges support from the Swedish Research Council (VR) and the Carl Trygger Foundation (CTS). K.R. has received support from the Norwegian Research Council through a Strategic University Program in Quantum Chemistry (Grant No 154011/420), and the NANOMAT program (Grant No. 158538/431). Computational resources were provided by National Supercomputing Center, Linköping, the Center for Parallel Computers, Stockholm, and The High Performance Computing Program of the University of Tromsø.

[1] J. E. Harriman, *Theoretical Foundations of Electron Spin Resonance* (Academic, New York, 1978).
[2] N. M. Atherton, *Principles of Electron Spin Resonance*, 2nd ed. (Ellis Horwood, New York, 1993).
[3] T. Kawamura, S. Matsunami, and T. Yonezawa, Bull. Chem. Soc. Jpn. **40**, 1111 (1967).
[4] T. Kawamura, S. Matsunami, T. Yonezawa, and K. Fukui, Bull. Chem. Soc. Jpn. **38**, 1935 (1965).
[5] K. Umemoto, Y. Deguchi, and H. Takaki, Bull. Chem. Soc. Jpn. **36**, 560 (1963).
[6] V. I. Krinichnyi, O. Ya. Grinberg, V. R. Bogatyrenko, G. I. Likhtenshtein, and Ya. S. Lebedev, Biophysics (Engl. Transl.) **30**, 233 (1985).
[7] M. A. Ondar, O. Ya. Grinberg, A. A. Dubinskii, and Ya. S. Lebedev, Sov. J. Chem. Phys. **3**, 781 (1985).
[8] I. Al-Bala'a and R. D. Bates, Jr., J. Magn. Reson. (1969-1992) **73**, 78 (1987).
[9] S. Moon, S. Patchkovskii, and D. R. Salahub, J. Mol. Struct.: THEOCHEM **632**, 287 (2003).
[10] B. Minaev, O. Loboda, O. Vahtras, K. Ruud, and H. Ågren, Theor. Chem. Acc. **111**, 168 (2004).
[11] N. Rega, M. Cossi, and V. Barone, J. Chem. Phys. **105**, 11060 (1996).
[12] B. Fernández, O. Christiansen, O. Bludsky, P. Jørgensen, and K. V. Mikkelsen, J. Chem. Phys. **104**, 629 (1996).
[13] M. Kaupp, Biochemistry **41**, 2895 (2002).
[14] M. Kaupp, C. Remenyi, J. Vaara, O. L. Malkina, and V. G. Malkin, J. Am. Chem. Soc. **124**, 2709 (2002).
[15] K. M. Neyman, G. I. Ganyushin, Z. Rinkevicius, and N. Rösch, Int. J. Quantum Chem. **90**, 1404 (2003).
[16] M. Engström, F. Himo, A. Gräslund, B. Minaev, O. Vahtras, and H. Ågren, J. Phys. Chem. A **104**, 5149 (2000).
[17] M. Engström, O. Vahtras, and H. Ågren, Chem. Phys. Lett. **328**, 483 (2000).
[18] R. Owenius, M. Engström, M. Lindgren, and M. Huber, J. Phys. Chem. A **105**, 10967 (2001).
[19] M. Engström, J. Vaara, B. Schimmelpfennig, and H. Ågren, J. Phys. Chem. B **106**, 12354 (2002).
[20] I. Ciofini, R. Reviakine, A. Arbuznikov, and M. Kaupp, Theor. Chem. Acc. **111**, 132 (2004). This paper describes the use of the CPCM formalism for electronic $g$-tensor calculations and appeared in the final stages in the preparation of this article.
[21] A. J. Stone, Mol. Phys. **6**, 509 (1963); **7**, 311 (1964).
[22] M. Knüpling, J. T. Töring, and S. Un, Chem. Phys. **219**, 291 (1997).
[23] Z. Rinkevicius, L. Telyatnyk, P. Salek, O. Vahtras, and H. Ågren, J. Chem. Phys. **119**, 10489 (2003).
[24] S. Miertus, E. Scrocco, and J. Tomasi, Chem. Phys. **55**, 117 (1981).
[25] R. Improta and V. Barone, Chem. Rev. (Washington, D.C.) **104**, 1231 (2004).
[26] G. Schreckenbach and T. Ziegler, J. Phys. Chem. A **101**, 3388 (1997).
[27] O. L. Malkina, J. Vaara, B. Schimmelpfenning, M. Munzarová, V. G. Malkin, and M. Kaupp, J. Am. Chem. Soc. **122**, 9206 (2000).
[28] F. Neese, J. Chem. Phys. **115**, 11080 (2001).
[29] M. Kaupp, R. Reviakine, O. L. Malkina, A. Arbuznikov, B. Schimmelpfenning, and V. G. Malkin, J. Comput. Chem. **23**, 794 (2002).
[30] B. A. Hess, C. M. Marian, U. Wahlgren, and O. Gropen, Chem. Phys. Lett. **251**, 365 (1996).
[31] B. Schimmelpfennig, *AMFI: An Atomic Spin-Orbit Mean Field Integral Program* (University of Stockholm, Sweden, 1996).
[32] R. Cammi, L. Frediani, B. Mennucci, and K. Ruud, J. Chem. Phys. **119**, 5818 (2003).
[33] M. J. Frisch, G. W. Trucks, H. B. Schlegel *et al.*, GAUSSIAN 98, Revision A.7, Gaussian, Inc., Pittsburgh, PA, 1998.
[34] T. Helgaker, H. J. Aa. Jensen, P. Jørgensen *et al.*, DALTON, Release 1.2, 2001. See http://www.kjemi.uio.no/software/dalton/dalton.html
[35] E. Cancès, B. Mennucci, and J. Tomasi, J. Chem. Phys. **107**, 3032 (1997).
[36] A. D. Becke, Phys. Rev. A **38**, 3098 (1988).
[37] J. P. Perdew, Phys. Rev. B **33**, 8822 (1986).
[38] S. J. Vosko, L. Wilk, and M. Nusair, Can. J. Phys. **58**, 1200 (1980).
[39] C. Lee, W. Yang, and R. G. Parr, Phys. Rev. B **37**, 785 (1988).
[40] A. D. Becke, J. Chem. Phys. **98**, 5648 (1993).
[41] W. Kutzelnigg, U. Fleischer, and M. Schindler, in *NMR Basic Principles and Progress*, edited by P. Diehl, E. Fluck, H. Günther, R. Kosfeld, and J. Seelig (Springer, Heidelberg, 1990), Vol. 23, p. 165.
[42] S. Huzinaga, *Approximate Atomic Functions* (University of Alberta, Edmonton, 1971).
[43] B. Mennucci, J. Am. Chem. Soc. **124**, 1506 (2002).
[44] T. Yagi, H. Takase, K. Morihashi, and O. Kikucki, Chem. Phys. **232**, 1 (1998).
[45] R. Cammi, M. Cossi, B. Mennucci, and J. Tomasi, J. Chem. Phys. **105**, 10556 (1996).